

Electronic Supplementary Information

2D MOF nanosheets as an artificial light-harvesting system with enhanced photoelectric switching performance

Lin Liu,^{1,a} Xue-Ying Lu,^{1,a} Mei-Li Zhang,^{*a} Yi-Xia Ren,^a Ji-Jiang Wang,^a Xiao-Gang Yang^{*b}

^a Department of Chemistry and Chemical Engineering, Yan'an University, Laboratory of New Energy & New Function Materials, Yan'an, 716000, P. R. China.

^b College of Chemistry and Chemical Engineering, Luoyang Normal University, Luoyang 471934, P. R. China.

¹ Lin Liu and Xue-Ying Lu are co-first authors; they contributed equally to the work.

**Corresponding author. E-mail: yxg2233@126.com; ydzml2332041@163.com*

Table of Content

Materials and general procedures.	3
Synthesis of [Cd(ppda)(mbib)] (Cd-MOF).	4
Preparation of MOF nanosheets.	4
Preparation of working electrode.	4
Theoretical calculations.	5
Figure S1. Powder X-ray diffraction (PXRD) curve of Cd-MOF.	6
Figure S2. Thermo gravimetric curve of Cd-MOF.	7
Figure S3-7. Crystal structure of Cd-MOF.	8
Figure S8. PL spectra of ppda and mbib.	12
Figure S9. Fluorescence decay curve of ppda and mbib.	13
Figure S10-12. Density functional theory (DFT) calculation.	14
Figure S13. SEM images of Cd-MOF.	17
Figure S14. Powder X-ray diffraction (PXRD) curve of Cd-MOF 2D nanosheets.	18
Figure S15. UV-vis absorption and fluorescence spectra.	19
Figure S16. Stern–Volmer plot.	20
Figure S17. Fluorescence decay curves of 2D MOF nanosheets	21
Figure S18. Thermogravimetric analysis (TGA) curve of CM6@Cd-MOF.	22
Figure S19. SEM image and elemental distribution maps of of CM6@Cd-MOF.	23
Figure S20. CV curves of Cd-MOF and CM6@ Cd-MOF.	24
Figure S21. The UV-visible absorption spectra of Cd-MOF and CM6@Cd-MOF in solid state.	25
Table S1. Crystallographic data and experimental details for Cd-MOF.	26
Table S2. Selected bond distances /Å and bond angles /° for Cd-MOF.	27
Table S3. Comparisons of Cd-MOF with reported 2D materials for photocurrent performance.	28
References	29

A. Experimental Section

1. Materials and general procedures.

All the starting reagents and solvents were commercially available and used as received without further purification. The hydrothermal reaction was performed in a 25 mL Teflon-lined stainless steel autoclave under autogenous pressure. Elemental analyses for C, H, and N were carried out on a Flash 2000 organic elemental analyzer. Thermal gravimetric analyses (TGA) were carried out on a SDT Q600 thermogravimetric analyzer with a heating rate of 10 °C/min under a N₂ atmosphere. Powder X-ray diffraction (PXRD) measurements were performed on a Bruker D8-ADVANCE X-ray diffractometer with Cu K α radiation ($\lambda = 1.5418 \text{ \AA}$).

X-ray single-crystal diffraction data for Cd-MOF was collected on a Bruker Smart 1000 CCD area-detector diffractometer with Mo-K α radiation ($\lambda = 0.71073 \text{ \AA}$) by ω scan mode. The crystal structure was solved by direct methods, using SHELXS-2014 and least-squares refined with SHELXL-2014 using anisotropic thermal displacement parameters for all non-hydrogen atoms.^{1,2} Further details for structural analysis are summarized in Table S1. Selected bond distances and bond angles are listed in Table S2. CCDC No. 2153702 contain the supplementary crystallographic data for Cd-MOF. This material can be obtained free of charge via <http://www.ccdc.cam.ac.uk/conts/retrieving.html>, or from the Cambridge Crystallographic Data Centre, 12 Union Road, Cambridge CB2 1EZ, UK; fax: (+44) 1223-336-033; or E-mail: deposit@ccdc.cam.ac.uk.

UV-vis absorption spectra was measured using a Shimadzu UV-3600 plus UV-vis-NIR spectrophotometer. Room temperature photoluminescence (PL) spectra and time-resolved lifetime were conducted on an Edinburgh FLS1000 fluorescence spectrometer equipped with a xenon arc lamp (Xe900) and nanosecond flash-lamp (nF900). The morphology of the nanosheets were performed by a field emission scanning electron microscope (SEM Sigma 500). The thickness of nanosheets were tested by a Bruker multimode 8 atomic force microscope (AFM).

Time-dependent photocurrent density curves and electrochemical impedance spectroscopy Nyquist plots were measured by a CHI 660E electrochemical analyzer (CH Instruments, Chenhua Co., Shanghai, China) in a standard three-electrode system. Powder of Cd-MOF and CM6@Cd-MOF modified indium tin oxide (ITO) as the working electrode (working area of 1.0 cm²), Ag/AgCl as a reference electrode, a platinum wire electrode as a counter electrode, and 0.5 M sodium sulfate aqueous solution as electrolyte. The system was irradiated by a 300 W Xe lamp. Wavelength-dependent photocurrent density curves were tested by MPI-EO PEC analysis system (Xi'an Remex Analysis Instrument Co., Ltd., Xi'an, China). The monochromatic light was generated by a 300 W Xe arc lamp assembled with a Omni-λ150 monochromator.

2. Synthesis of [Cd(ppda)(mbib)] (Cd-MOF).

A mixture of H₂ppda (0.0210 g, 0.1 mmol), Cd(NO₃)₂·4H₂O (0.0308 g, 0.10 mmol), mbib (0.0194 g, 0.1 mmol) and KOH (5.6 mg, 0.1 mmol) were added to water (12 mL) in a 25 mL Teflon-lined stainless steel vessel. The mixture was heated at 160 °C for 72 h. After the reactive mixture was slowly cooled to room temperature, colourless block crystal of Cd-MOF was obtained. Elemental analysis calcd. (%) for C₂₄H₂₂CdN₄O₄: C 50.10, H 4.08, N 10.38; found (%): C 49.70, H 3.83, N 9.83.

3. Preparation of MOF nanosheets.

5 mg of Cd-MOF powder was dispersed in 20 ml of EtOH and sonicated 30 minutes. Then the sample was centrifuged at 8000 rpm, affording uniform MOF suspension. The integration of CM6@Cd-MOF suspension was prepared by gradual addition of CM6 EtOH solution (Total 360 μl, 2 μl each time) into 10 ml MOF suspension with intense stirring. The Cd-MOF and CM6@Cd-MOF nanosheets in solid can be obtained by dropping above suspension on indium tin oxide (ITO) or silicon wafer substrate and dried in air.

4. Preparation of working electrode.

The working electrodes were prepared by dropping the Cd-MOF or CM6@Cd-MOF EtOH suspension (0.2 mL) onto the surface of the pre-treated indium tin oxide (ITO) substrate ($1 \times 4 \text{ cm}^2$) by controlling the coating area about 1 cm^2 , and allowing it to dry at room temperature. The ITO substrate was washed by ethanol, and water under ultrasonic processing for about 30 min then dried in natural environment.

5. Theoretical calculations.

The density functional theory (DFT) calculations were conducted on Material Studio software package³ Dmol3 module.⁵ The structure mode was obtained by removing the symmetry of the crystallographic information file (cif) of the title MOF, remaining part of organic molecules and one metal ion. Full optimization of initial configuration were handled by Perdew-Wang (PW91)⁶ generalized gradient approximation (GGA) method.

B. Supporting Figures

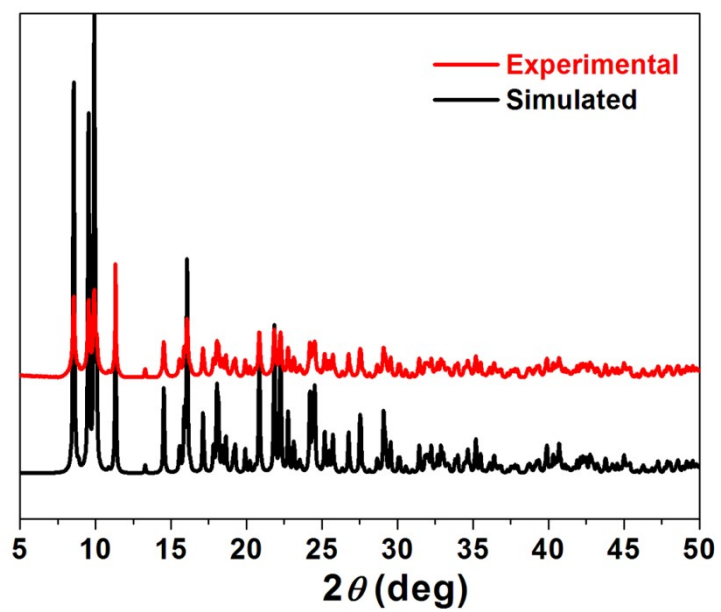


Figure S1. Powder X-ray diffraction (PXRD) curve of Cd-MOF.

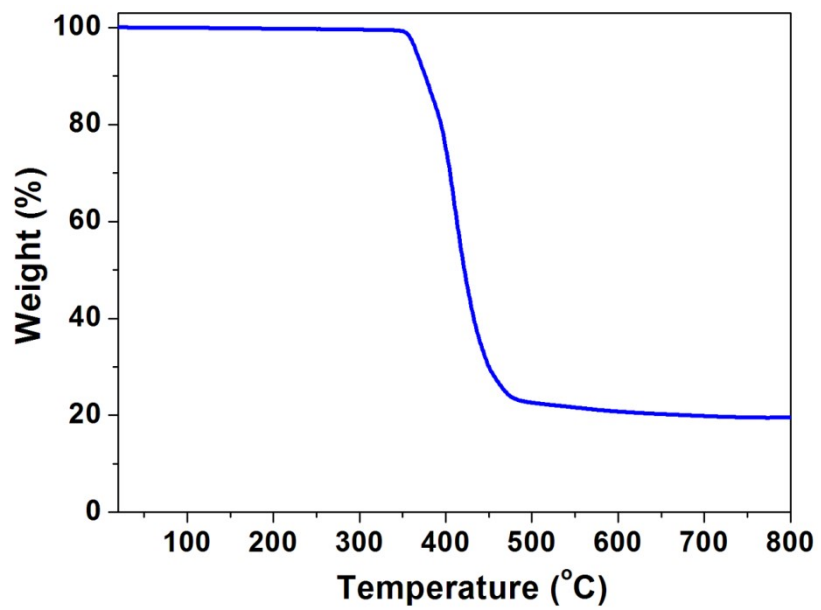
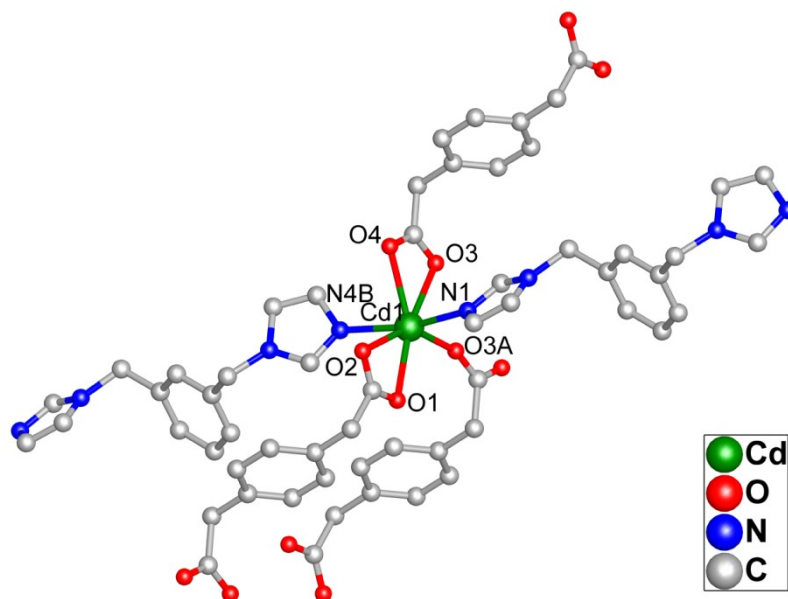
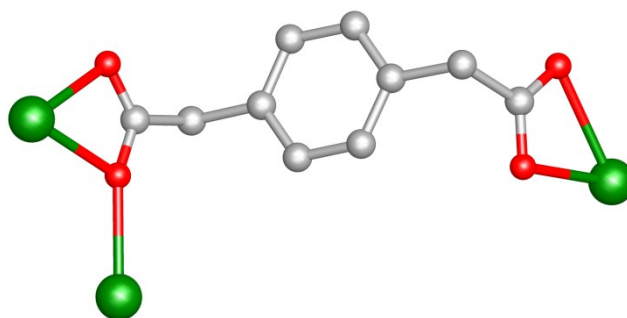


Figure S2. Thermogravimetric analysis (TGA) curve of Cd-MOF.



(a)



(b)

Figure S3. (a) View of local coordination environment of Cd(II) ion in Cd-MOF. Symmetry codes: A = $-x, -y+2, -z+1$; B = $x, y+1, z-1$. (b) The coordination mode of ppda ligand in Cd-MOF.

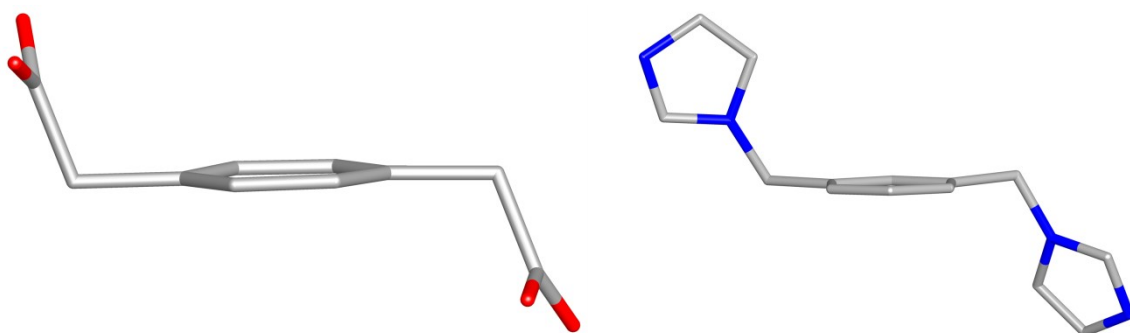


Figure S4. Side view of the *trans*-conformation of ppda and mbib ligands in Cd-MOF.

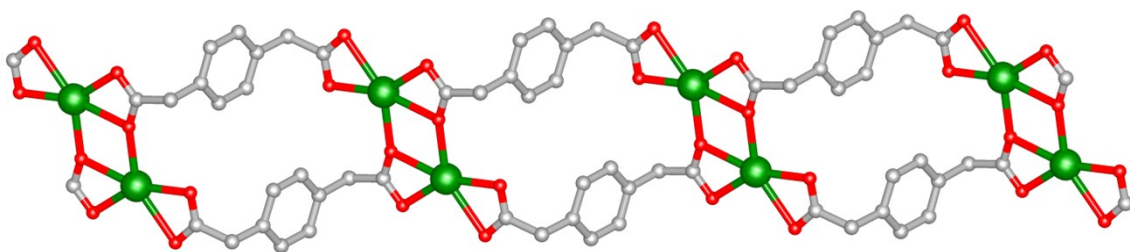
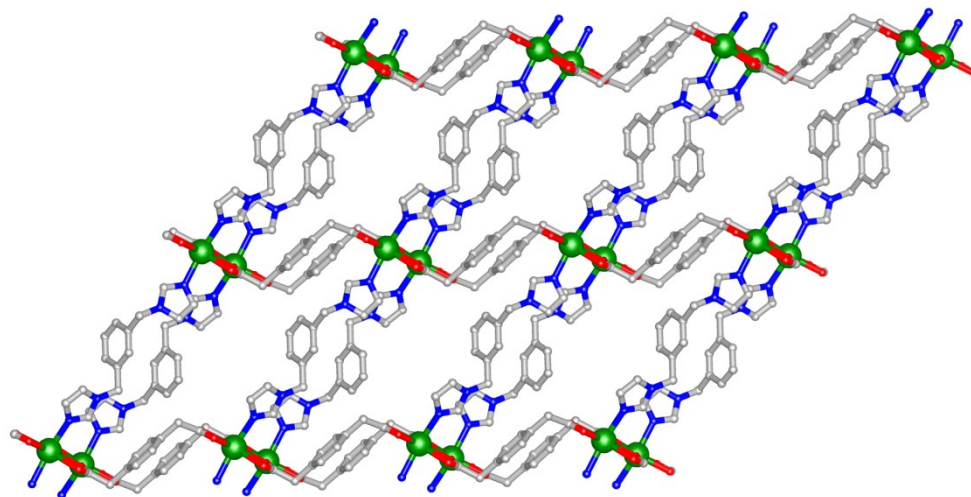
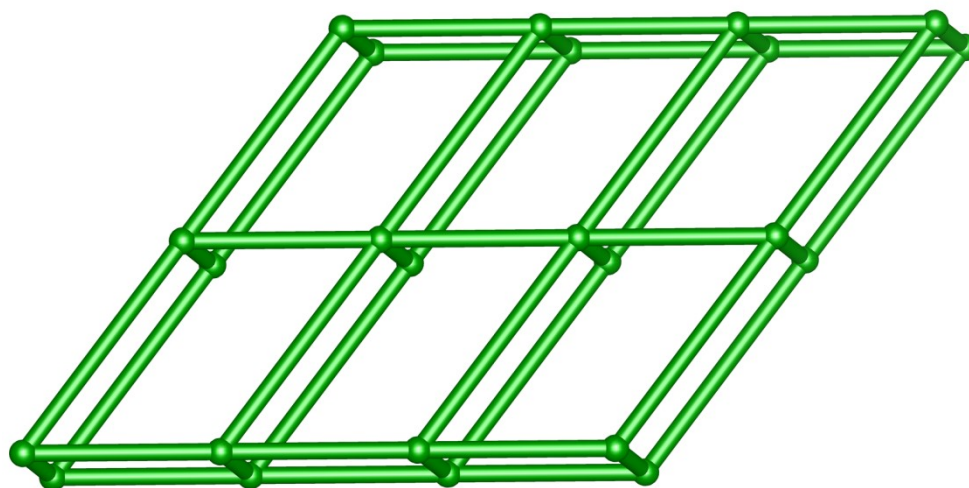


Figure S5. View of the 1D double strand chain of Cd-MOF assembled by dinuclear Cd(II) units and ppda ligands.



(a)



(a)

Figure S6. Ball-and-stick (a) and schematic representation (b) view of the 2D double layer structure of Cd-MOF. The dinuclear Cd(II) units are simplified as nodes, ppda and mbib ligands are simplified as linkers.

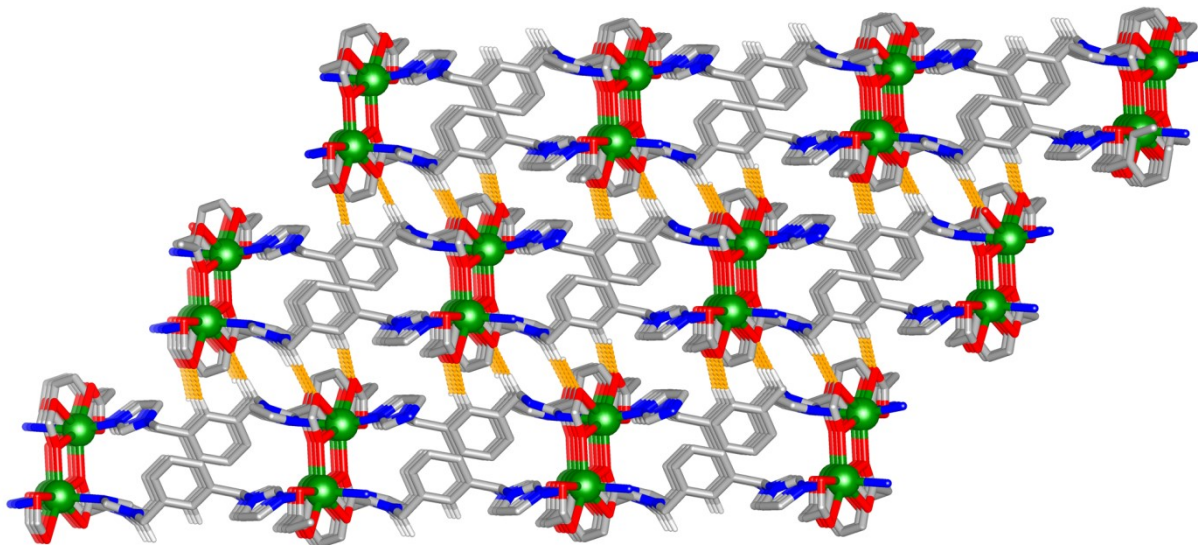
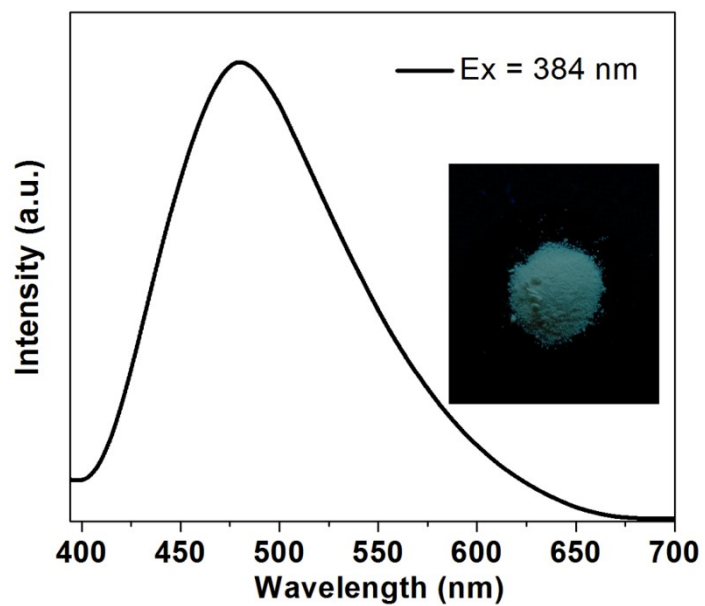
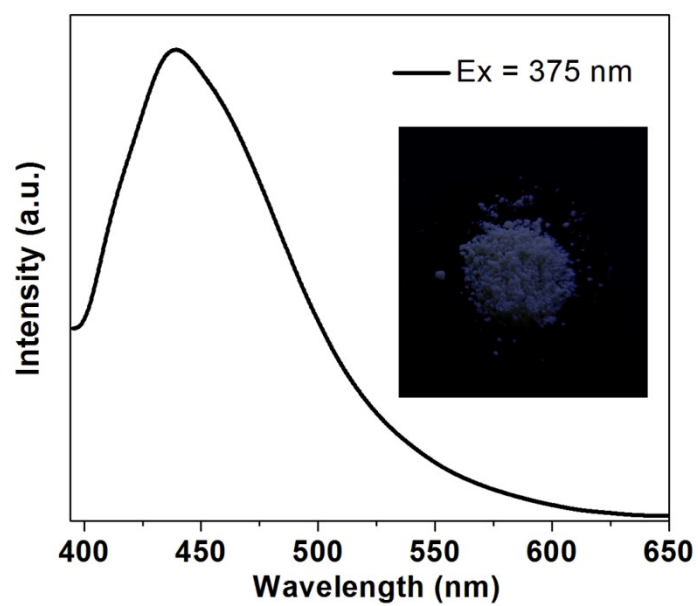


Figure S7. C–H \cdots O (C16–H16 \cdots O2, C21–H21 \cdots O4) hydrogen bonds between the adjacent 2D double layers.

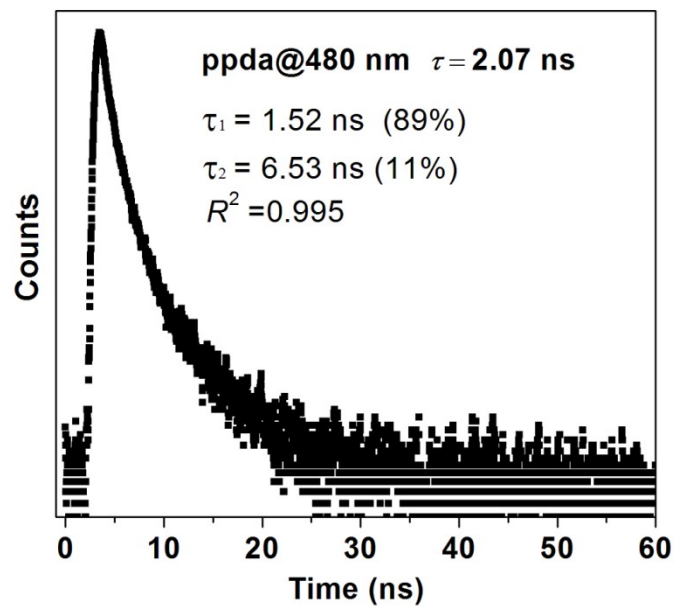


(a)

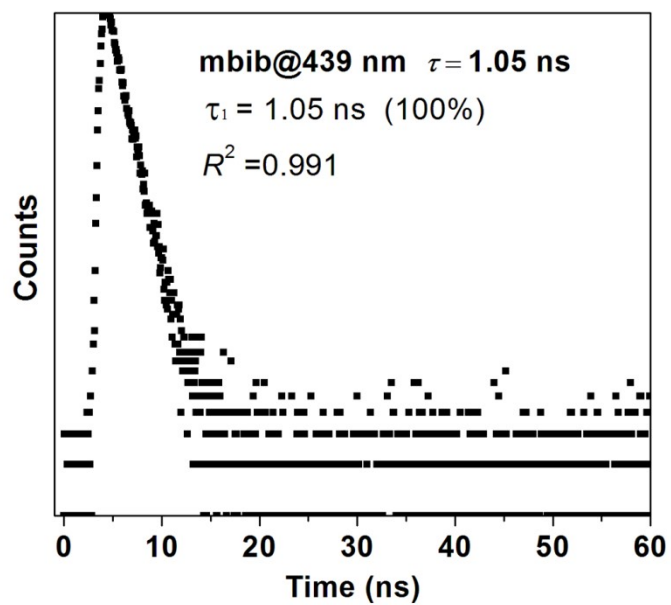


(b)

Figure S8. Emission spectra of ppda (a) and mbib (b) in solid state measured at room temperature. Inset shows the solid state samples of ppda and mbib under UV light radiation.



(a)



(b)

Figure S9. Fluorescence decay curve of ppda (a) and mbib (b) in solid state measured at room temperature.

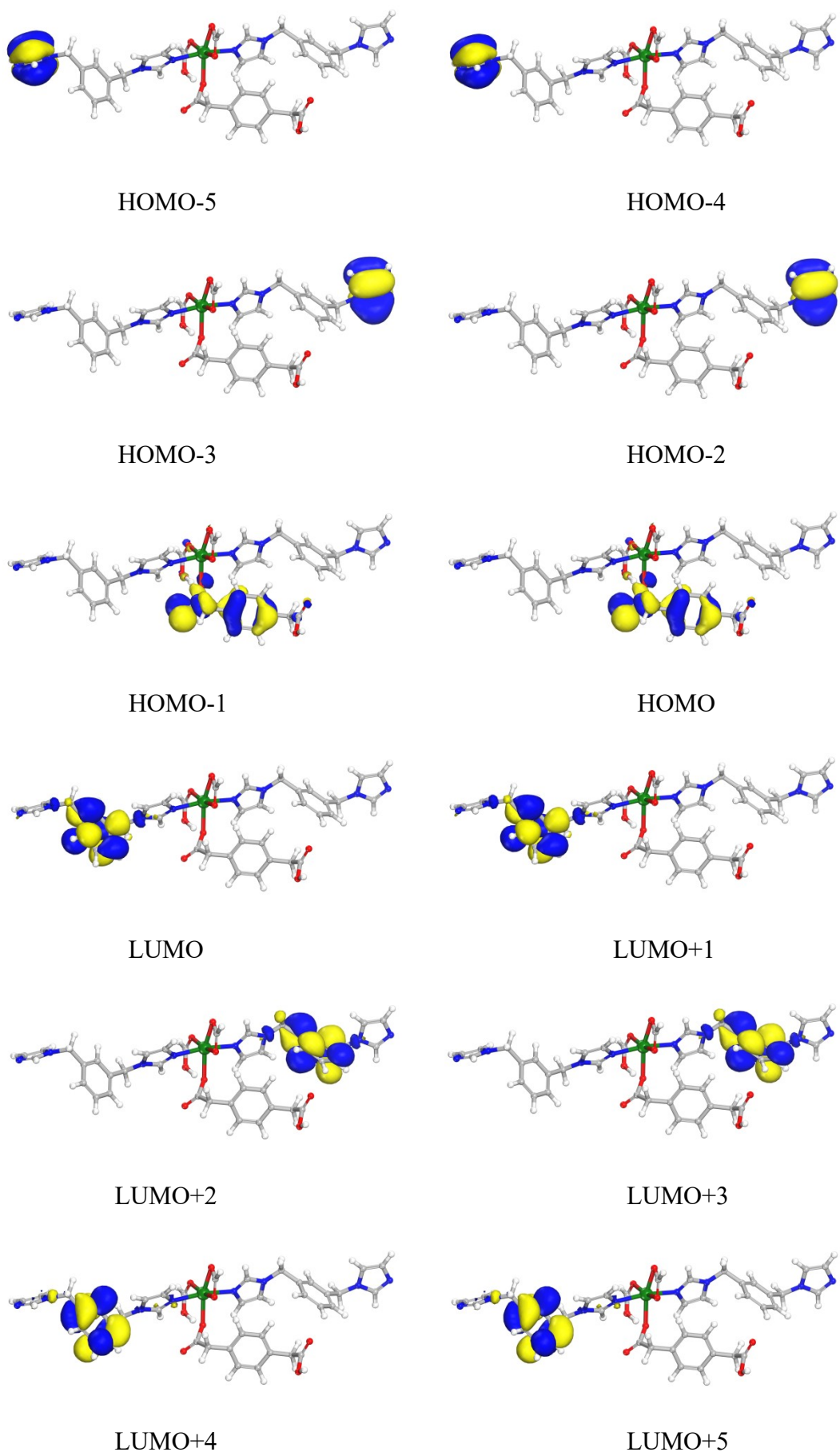


Figure S10. View of HOMOs and LUMOs for the DFT optimized structure of Cd-MOF.

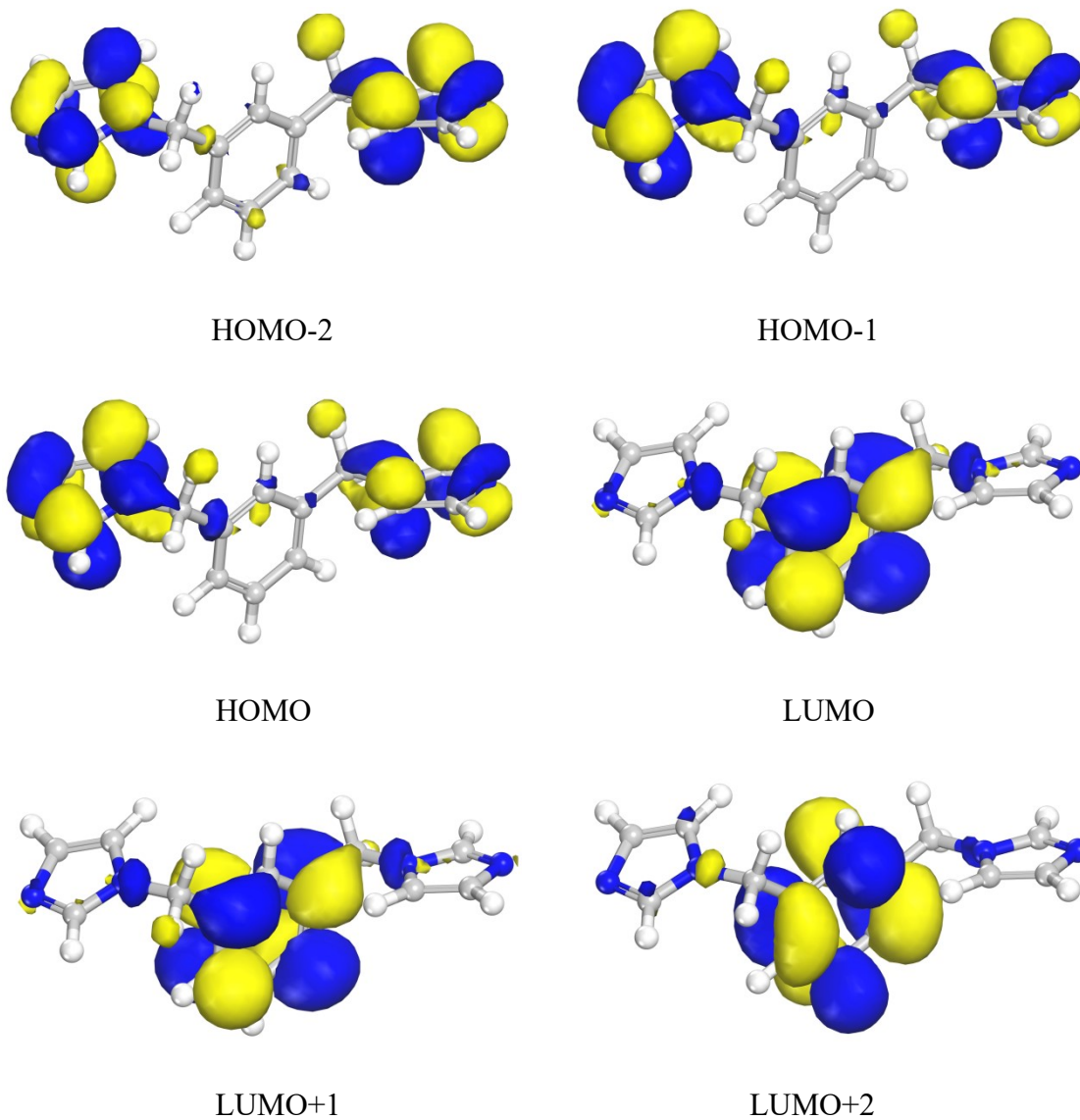


Figure S11. View of HOMOs and LUMOs for the DFT optimized structure of mbib.

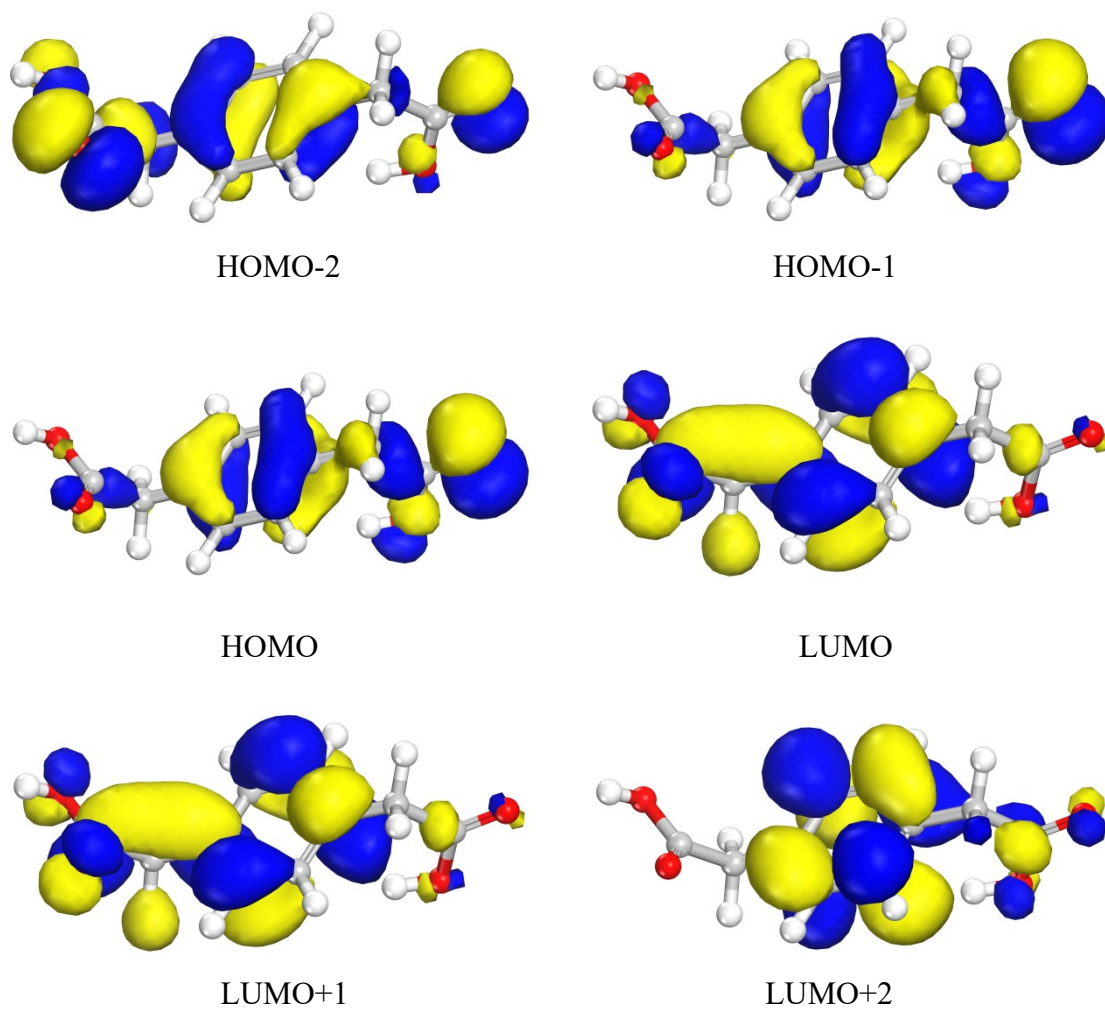


Figure S12. View of HOMOs and LUMOs for the DFT optimized structure of ppda.

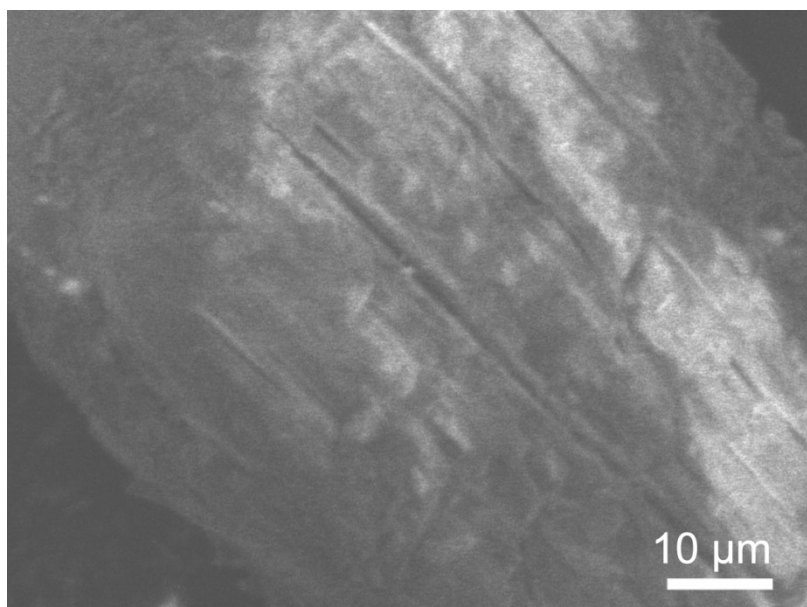
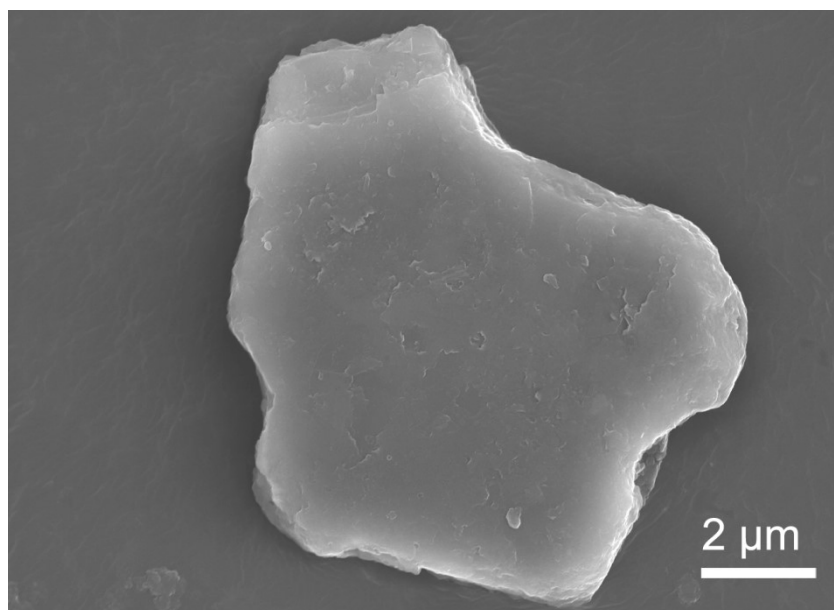


Figure S13. Top (a) and side (b) view of SEM images of Cd-MOF bulk crystal with layered structure.

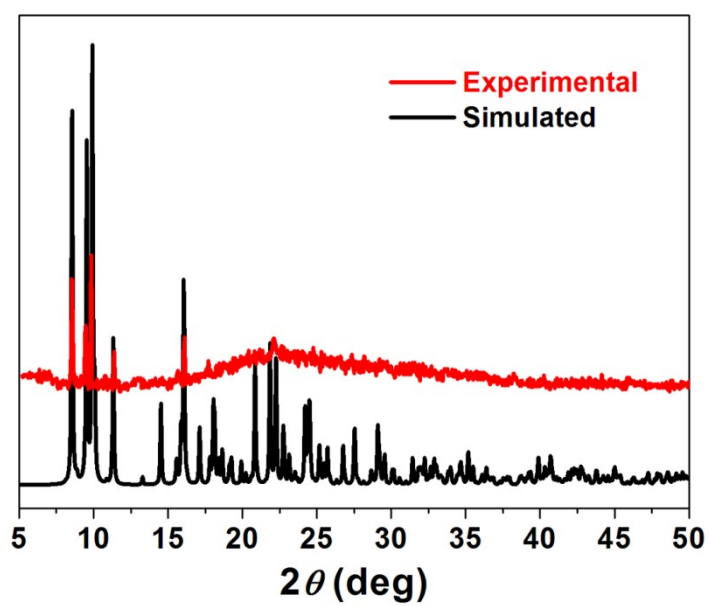


Figure S14. Powder X-ray diffraction (PXRD) curve of Cd-MOF 2D nanosheets.

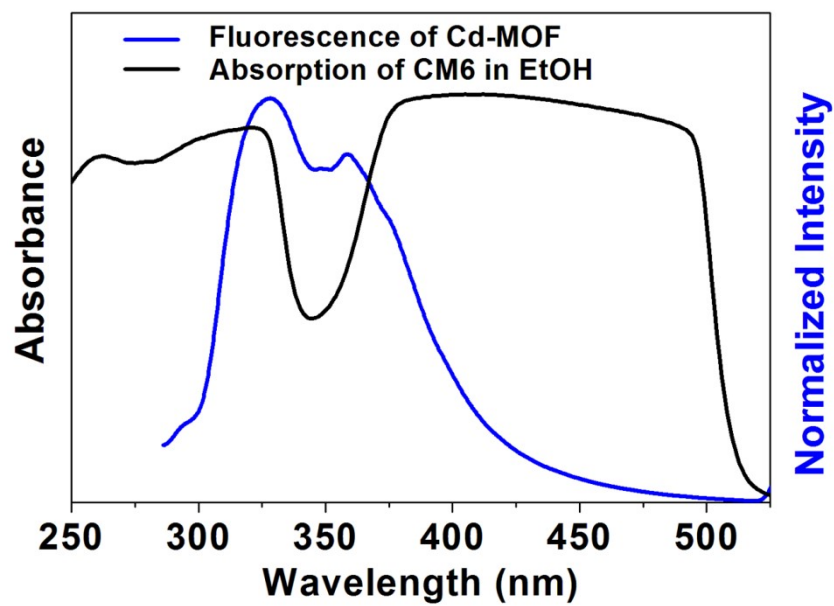


Figure S15. Normalized UV-vis absorption of CM6 and fluorescence spectra of Cd-MOF nanosheets dispersed in ethanol. The absorption spectra of free CM6 was measured in EtOH.

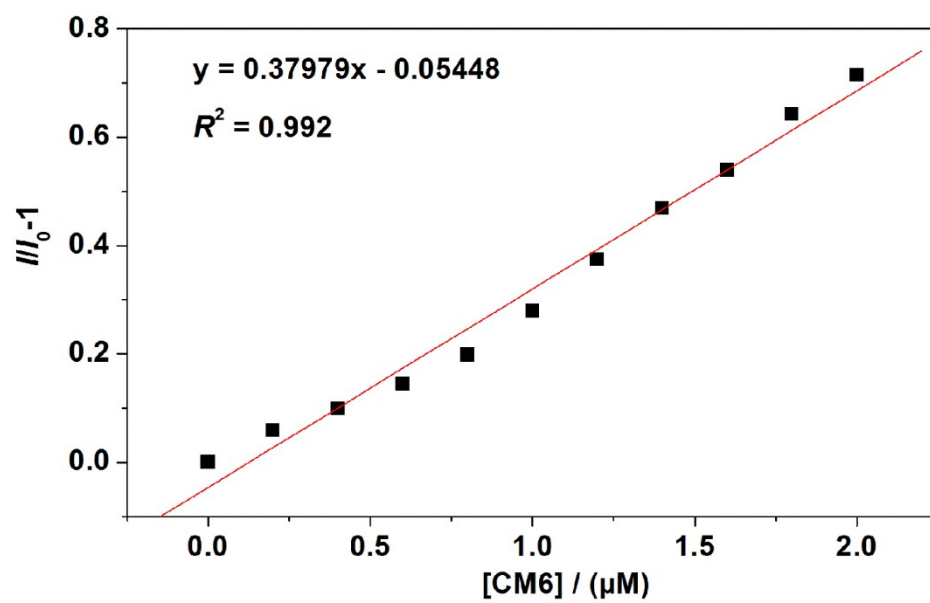


Figure S16. Stern–Volmer plot of nanosheets suspension quenched by coumarin 6 (CM6).

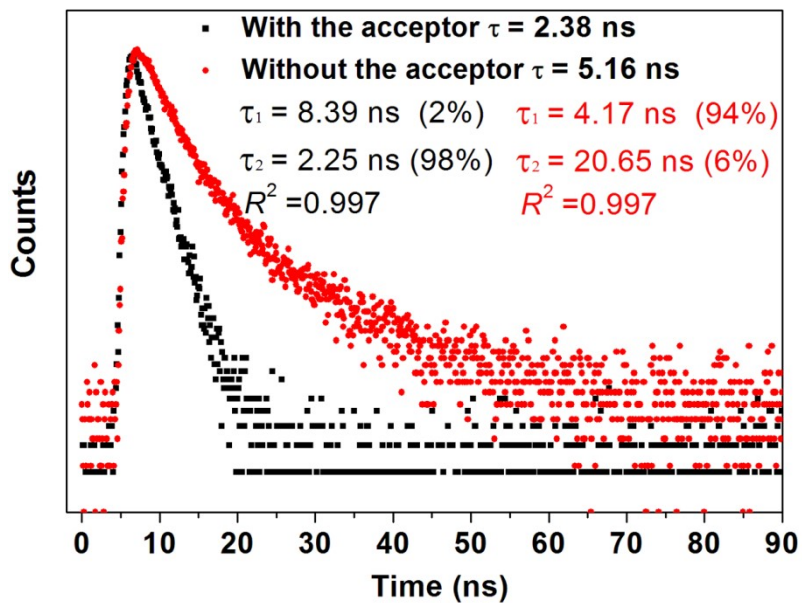


Figure 17. Fluorescence decay curves of Cd-MOF nanosheets donor dispersed in ethanol in the presence and absence of an CM6 acceptor.

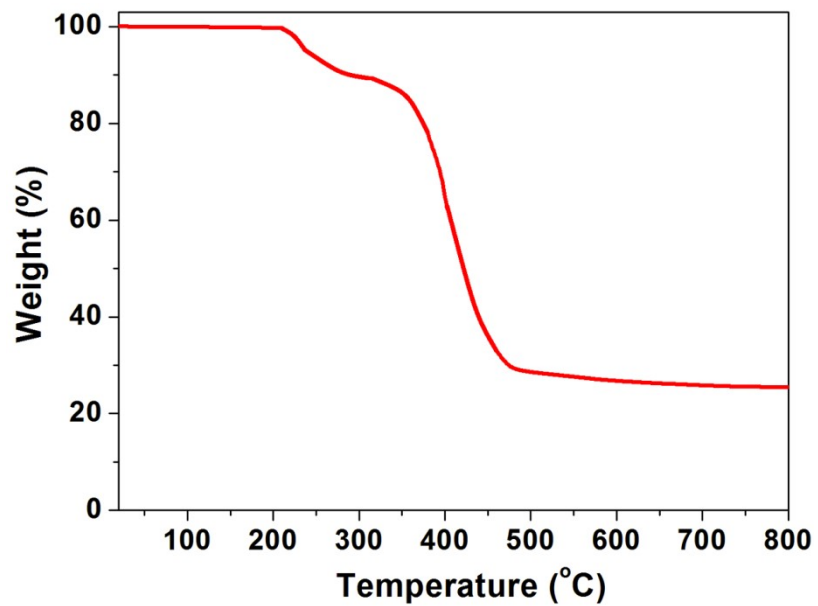


Figure 18. Thermogravimetric analysis (TGA) curve of CM6@Cd-MOF.

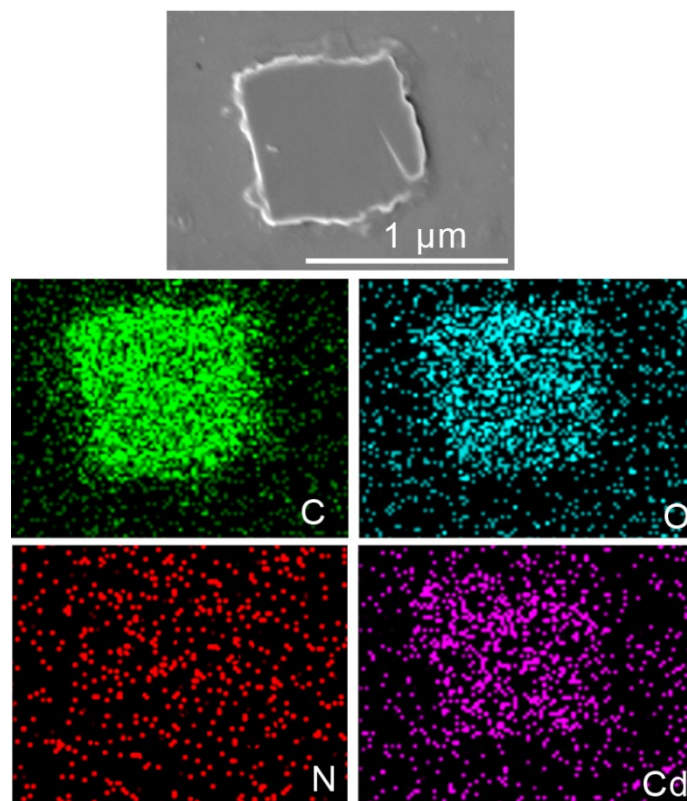


Figure S19. SEM image and elemental distribution maps of C, N, O and Cd of CM6@Cd-MOF.

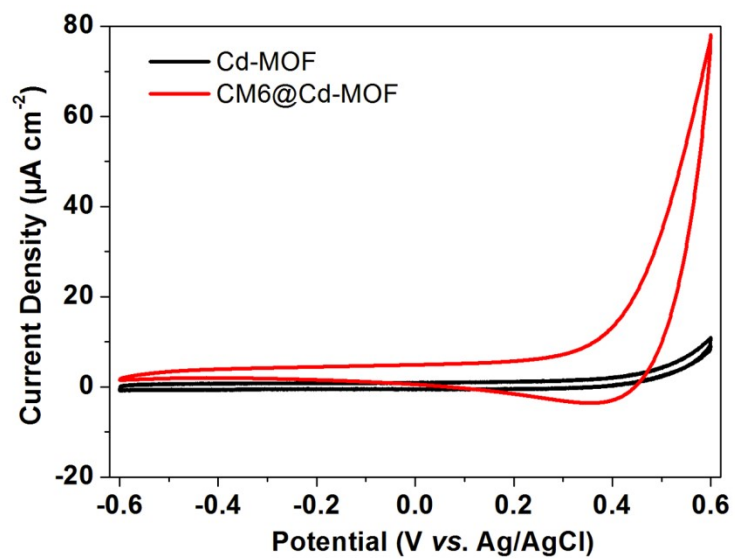
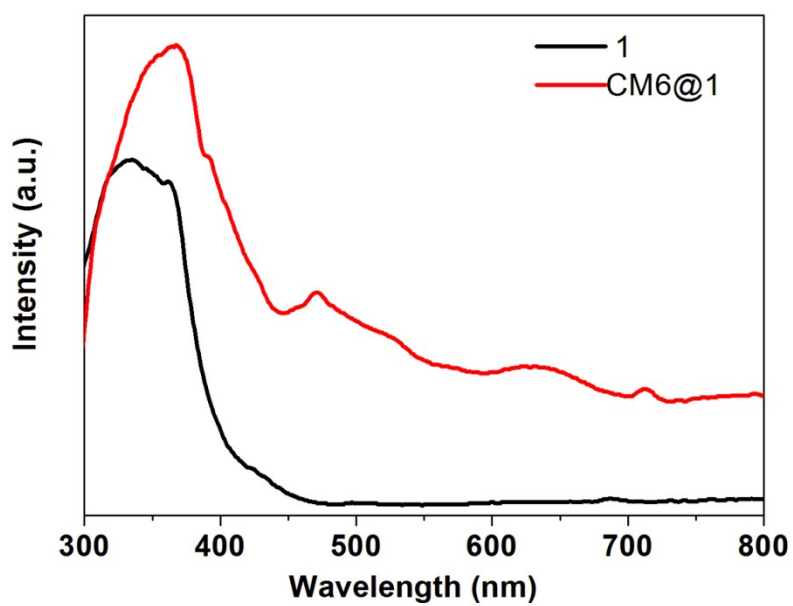
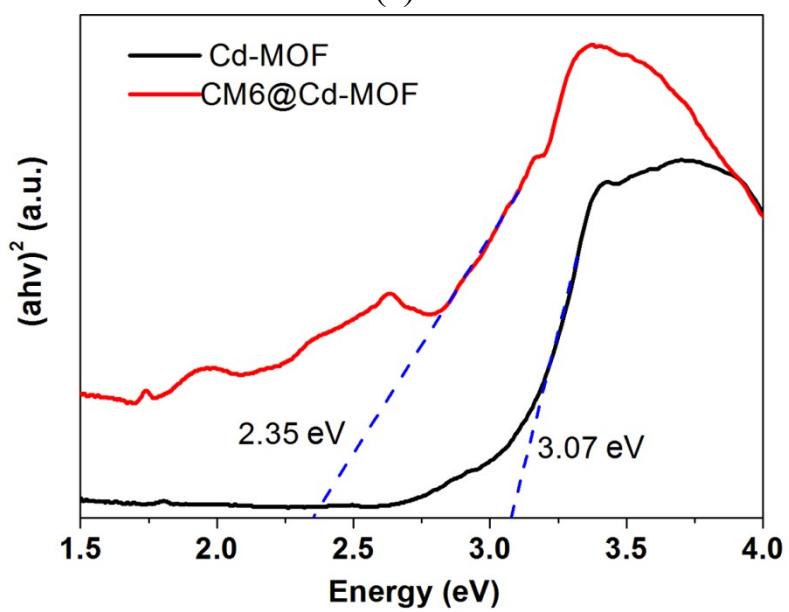


Figure S20. CV curves of Cd-MOF and CM6@ Cd-MOF tested in 0.5 M Na_2SO_4 aqueous solution.



(a)



(b)

Figure S21. The UV-visible absorption spectra (a) and Tauc plots (b) of Cd-MOF and CM6@Cd-MOF measured in solid state.

C. Supporting Tables

Table S1. Crystallographic data and experimental details for Cd-MOF.

Complex	Cd-MOF
Formula	C ₂₄ H ₂₂ CdN ₄ O ₄
Mass	542.85
Crystal system	Triclinic
Space group	<i>P</i> $\bar{1}$
<i>a</i> (Å)	11.0962(6)
<i>b</i> (Å)	11.3601(6)
<i>c</i> (Å)	11.4294(6)
α (°)	86.8290(10)
β (°)	61.8360(10)
γ (°)	67.0680(10)
<i>V</i> (Å ³)	1154.99(11)
<i>Z</i>	2
<i>D_c</i> (g cm ⁻³)	1.561
μ (mm ⁻¹)	0.983
<i>R</i> _{int}	0.0080
Goof	1.234
<i>R</i> ₁ ^a / <i>wR</i> ₂ ^b [<i>I</i> > 2σ(<i>I</i>)]	0.0242/0.0632
<i>R</i> ₁ ^a / <i>wR</i> ₂ ^b (<i>all data</i>)	0.0260/0.0645

^a*R*₁ = Σ||*F*_o| - |*F*_c||/Σ|*F*_o|, *wR*₂ = [Σ*w*(*F*_o² - *F*_c²)²/Σ*w*(*F*_o²)²]^{1/2}

Table S2. Selected bond distances /Å and bond angles /° for Cd-MOF.

Cd(1)-N(1)	2.2947(19)	Cd(1)-O(1)	2.3357(18)
Cd(1)-N(4)#2	2.3543(18)	Cd(1)-O(2)	2.5651(18)
Cd(1)-O(3)#1	2.3445(18)	Cd(1)-O(4)	2.4776(19)
Cd(1)-O(3)	2.4725(18)		
N(1)-Cd(1)-O(1)	96.12(7)	N(1)-Cd(1)-O(3)#1	94.72(8)
N(1)-Cd(1)-N(4)#2	166.05(8)	O(1)-Cd(1)-N(4)#2	89.38(7)
O(1)-Cd(1)-O(3)#1	92.95(7)	O(3)#1-Cd(1)-N(4)#2	97.80(7)
O(3)#1-Cd(1)-O(3)	68.21(7)	O(3)#1-Cd(1)-O(3)	68.21(7)
O(3)-Cd(1)-O(4)	51.74(6)	O(3)-Cd(1)-O(4)	51.74(6)
N(1)-Cd(1)-O(3)	86.76(7)	O(1)-Cd(1)-O(3)	161.13(7)
N(4)#2-Cd(1)-O(3)	92.18(7)	N(1)-Cd(1)-O(4)	85.24(8)
O(3)#1-Cd(1)-O(4)	119.89(6)	N(4)#2-Cd(1)-O(4)	83.20(7)
N(1)-Cd(1)-O(2)	88.35(7)	O(1)-Cd(1)-O(2)	53.02(6)
N(4)#2-Cd(1)-O(2)	84.73(7)	O(3)-Cd(1)-O(2)	145.84(6)
O(4)-Cd(1)-O(2)	94.17(6)		

Symmetry code: #1: -x,-y+2,-z+1; #2: x,y+1,z-1; #3: x+1,y,z-1; #4: x,y-1,z+1; #5: x-1,y,z+1.

Table S3. Comparisons of Cd-MOF with reported 2D materials for photocurrent performance.

Materials	Electrolyte	Photocurrent ($\mu\text{A cm}^{-2}$) without bias potential	$I_{\text{on}}/I_{\text{off}}$	Refs.
Cd-MOF	0.5 M Na_2SO_4	2.0	1000	This work
CM6@Cd-MOF	0.5 M Na_2SO_4	0.09	30	This work
Zn(II)-TBAPy MOF	0.5 M Na_2SO_4	4.492	37.55	7
Mn(II)-TBAPy	0.5 M Na_2SO_4	0.8	13	8
DMP@Mn(II)-TBAPy	0.5 M Na_2SO_4	4.8	160	8
Black phosphorus	0.1 M KOH	0.2265	264	9
AD-TMA	0.5 M Na_2SO_4	27.79	13 895	10
ACNNM	0.01 M KCl	0.1	5000	11
Graphdiyne	0.1 M KOH,	0.08	—	12
2D Se nanoflakes	0.1 M KOH	1.28	—	13
Squaraine- SnO_2	1 M NaNO_3	2.6	—	14
[Zn(5-BIPA)(phen)]	0.5 M Na_2SO_4	1.075	228	15
[Zn(4-BIPA)(phen)]	0.5 M Na_2SO_4	0.248	49	15

D. Supporting References

1. CrysAlisPro, Rigaku Oxford Diffraction, Version 1.171.39.6a.
2. G. M. Sheldrick, A short history of SHELX, *Acta Crystallogr. Sect. A*, 2008, **64**, 112.
3. B. Delley, An all-electron numerical method for solving the local density functional for polyatomic molecules, *J. Chem. Phys.*, 1990, **92**, 508-517.
4. B. Delley, From molecules to solids with the DMol³ approach, *J. Chem. Phys.*, 2000, **113**, 7756.
5. Dmol³ Module, MS Modeling, Version 2.2; Accelrys Inc.: San, Diego, 2003.
6. J. P. Perdew, J. A. Chevary, S. H. Vosko, K. A. Jackson, M. R. Pederson, D. J. Singh and C. Fiolhais, Atoms, molecules, solids, and surfaces: Applications of the generalized gradient approximation for exchange and correlation, *Phys. Rev. B*, 1992, **46**, 6671.
7. J. H. Qin, Y. D. Huang, Y. Zhao, X. G. Yang, F. F. Li, C. Wang and L. F. Ma, Highly dense packing of chromophoric linkers achievable in a pyrene-based metal-organic framework for photoelectric response, *Inorg. Chem.*, 2019, **58**, 15013–15016.
8. X. G. Yang, J. H. Qin, Y. D. Huang, Z. M. Zhai, L. F. Ma, D. Yan, Highly enhanced UV-vis-NIR light harvesting and photoelectric conversion of pyrene MOF by encapsulation of D- π -A cyanine dye, *J. Mater. Chem. C*, 2020, **8**, 17169–17175.
9. X. Ren, Z. Li, Z. Huang, D. Sang, H. Qiao, X. Qi, J. Li, J. Zhong, H. Zhang, Environmentally robust black phosphorus nanosheets in solution: application for self-powered photodetector. *Adv. Funct. Mater.*, 2017, **27**, 1606834.
10. X. G. Yang, Z. M. Zhai, X. M. Lu, L. F. Ma, D. Yan, Fast crystallization-deposition of orderly molecule level heterojunction thin films showing tunable up-conversion and ultrahigh photoelectric response, *ACS Cent. Sci.*, 2020, **6**, 1169–1178.
11. K. Xiao, B. Tu, L. Chen, T. Heil, L. Wen, L. Jiang, M. Antonietti, Photo-driven ion transport for photodetector based on asymmetric carbon nitride nanotube membrane. *Angew. Chem. Int. Ed.*, 2019, **58**, 12574–12579.

12. Y. Zhang, P. Huang, J. Guo, R. Shi, W. Huang, Z. Shi, L. Wu, F. Zhang, L. Gao, C. Li, X. Zhang, J. Xu, H. Zhang, Graphdiyne-based flexible photodetectors with high responsivity and detectivity, *Adv. Mater.*, 2020, 2001082.
13. T. Fan, Z. Xie, W. Huang, Z. Li, H. Zhang, Two-dimensional non-layered selenium nanoflakes: facile fabrications and applications for self-powered photo-detector, *Nanotechnology*, 2019, **30**, 114002.
14. K. Liang, K.-Y. Law, D. G. Whitten. Synthesis, characterization, photophysics, and photosensitization studies of squaraine-bipyridinium diads. *J. Phys. Chem. B*, 1997, **101**, 540–546.
15. X. G. Yang, X. M. Lu, Z. M. Zhai, J. H. Qin, X. H. Chang, M. L. Han, F. F. Li and L. F. Ma, π -Type halogen bonding enhanced long-last room temperature phosphorescence of Zn(II) coordination polymers for photoelectron response applications. *Inorg. Chem. Front.*, 2020, **7**, 2224–2230.